www.lajss.org
Latin American Journal of Solids and Structures 6 (2009) 73–87

On geometrical effects in micro-resonators

Claudia Comi

Department of Structural Engineering, Politecnico di Milano,
Piazza L. da Vinci 32, 20133 - Milano (Italy)

Abstract

The paper aanalyzes the nonlinear dynamic response of microresonators. A simple physical model of a single span beam axially constrained at both end, possibly with elastic constraints, is considered as representative of different common layout of microresonators. An analytical model, based on the Hamilton's principle, accounting for large displacements is presented and validated thanks to numerical finite element analyses. In order to widen the linear operation range of the device an optimal geometry of the resonator is proposed.

Keywords: MEMS, microresonator, nonlinear dynamics.

1 Introduction

Microresonators are currently used in various microelectromechanical devices (MEMS) such as accelerometers [1], [8], [5], pressure sensors [4] and strain transducers [11]. In resonant sensors the quantity to be measured produces a shift of the resonance frequency which can be recorded. Resonant sensing, with respect to others sensing principles, has the advantage of direct frequency output, high potential sensitivity and large dynamic range. The growing need of low cost devices imposes a drastic size reduction of these sensors. To maintain a good detectability and sensitivity, however, the maximum oscillation amplitude cannot be reduced proportionally. This implies that micro- and nano-resonators are often operated in the nonlinear regime.

Nonlinearities in electrostatically actuated resonators can have both mechanical and capacitive origin (see e.g. [6]). Mechanical nonlinearities in turn can be due to the material behavior and/or to geometrical effects. While material nonlinearities can usually be neglected in silicon microbeam resonators, mechanical nonlinearities related to large displacements play a significant role. Their effect increase as the size is reduced and hysteresis phenomena limit the allowable excitation range and quality factor of the resonator [1]. Electrostatic nonlinearities, on the other hand, are inherent to the actuation mechanism and they do not increase significantly as the size is reduced.

In the literature several complete formulations of nonlinear dynamics for plates, beam and cables are available, however, in the MEMS community, usually use is made of simplified one-degree of freedom models based on coarse assumptions on nonlinearities. The objective of

*Corresp. author email: claudia.comi@polimi.it Received 4 Nov 2008; In revised form 4 Mar 2009

the present work is to provide a rather simple but theoretically sound means the predict the nonlinear behaviour due to geometrical effects in microbeam resonators. In section 2 the theory of nonlinear oscillations (see e.g. [9], [10]) is reviewed and the Hamilton's principle is used as the basis of a one degree of freedom formulation. Explicit solutions for single span beams axially constrained by elastic springs are given and discussed. Besides the simplicity of the physical model several different dynamic behaviors consistent with real problems are obtained. In section 3 the nonlinear oscillation theory is applied to doubly clamped silicon microresonators and analytical results are compared with those obtained by a finite element electromechanical coupled analysis. Then a new geometry is proposed in order to enhance the range of dynamic linear behavior of the microresonator.

2 Nonlinear vibration of an axially loaded beam

2.1 Problem formulation

Consider a prismatic elastic beam with cross section A, momentum of inertia I and length L subject to an initial constant axial load P_0 and to a transversal distributed dynamic load $q\left(t,x\right)$, x being the coordinate along the beam axis and t the time. Let the longitudinal and transversal displacements of the beam axis be described by $u\left(x,t\right)$ and $w(x,t)$, respectively. The beam is axially constrained at both ends, possibly with elastic constraints represented by an axial spring of stiffness k_a at one end (see Figure 1).

The model here adopted for the description of the dynamic response of the beam is restricted by several hypotheses: (i) the beam is modeled by the Euler Bernoulli theory, (ii) variation of the cross section during vibration is neglected, (iii) stretching of the beam is small but finite (see e.g. [10] for details). With the above hypotheses, the axial strain along the beam axis reads

$$\varepsilon_0\left(x,t\right)=u'+\frac{1}{2}\left(w'\right)^2 \tag{1}$$

where a prime denotes spatial derivative with respect to the beam axis.

Denoting by E the material Young's modulus, the axial force N and the bending moment M can be expressed as

$$\begin{aligned} N\left(x,t\right)&=P_0+EA\left(u'+\frac{1}{2}\left(w'\right)^2\right)\\ M\left(x,t\right)&=EIw'' \end{aligned} \tag{2}$$

The equations of motion are readily derived by considering the equilibrium of forces acting on the differential segment of mass ρAdx of the deflected beam (see Figure 1)

$$\begin{aligned} N'-\rho A\ddot{u}&=0\\ M''-\left(Nw'\right)'+\rho A\ddot{w}&=q \end{aligned} \tag{3}$$

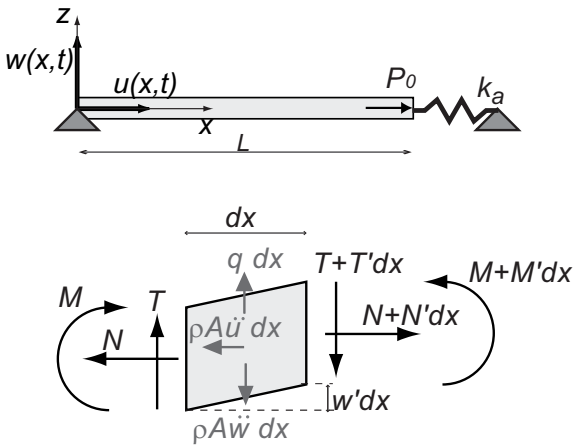

Figure 1: Scheme of the vibrating beam and free body diagram.

Introducing Eqs. (2) into Eqs. (3), one obtains a coupled differential system for the axial and transversal displacements u and w.

If inertial effects in the axial direction can be neglected, the problem decouples and one can obtain a differential equation in w only, as explained in the following. Setting to zero the longitudinal inertial force, from Eq. (3a), the axial force turns out to be a function of time only. From Eq. (2a) it follows

$$u' = \frac{N(t) - P_0}{EA} - \frac{1}{2}\left(w'\right)^2 \tag{4}$$

Integrating in space Eq.(4) with the boundary conditions

$$u(0,t) = 0, \quad u(L,t) = -\frac{N(t) - P_0}{k_a} \tag{5}$$

one obtains the axial force in the form

$$N(t) = P_0 + \frac{k_a EA}{k_a L + EA} \int_0^L \frac{1}{2}\left(w'\right)^2 dx \tag{6}$$

Note that the axial force has two contributions: the first one is due to a prestress $\frac{P_0}{A}$ acting on the beam, constant in time and independent from the beam transversal displacement w, while the second one is generated by the elongation of the beam induced by its finite deflection. This second contribution is present only in axially constrained beams. Substituting the axial force into the transversal dynamic equilibrium, Eq. (3b), the following nonlinear equation for the transverse beam oscillation is obtained

$$\left(EIw''\right)'' - P_0 w'' - \frac{k_a EA}{k_a L + EA} w'' \int_0^L \frac{1}{2}\left(w'\right)^2 dx + \rho A \ddot{w} = q \tag{7}$$

Table 1: Coefficients c and γ in Eq. (9) for single span beams with different boundary conditions

	c	γ
clamped-free	1.875	2.66
sliding-pinned	1.572	2.47
pinned-pinned	3.142	9.87
sliding-sliding	3.142	9.87
clamped-clamped	4.730	40.7

If the axial elongation is not constrained, the governing differential equation for the transverse displacement simplifies to:

$$\left(EIw''\right)'' - P_0 w'' + \rho A \ddot{w} = q \tag{8}$$

This latter equation has been widely studied in the literature and several solutions are available. The presence of a constant axial load P_0 changes the natural circular frequencies of the beam oscillation. For a single span beam, frequencies increase in the case of a tensile load and decrease in the case of a compressive load. The first resonant circular frequency ω_0 can be expressed as (cfr e.g. [3], [9], [5])

$$\omega_0\left(P_0\right) = \frac{c^2}{L^2}\sqrt{\frac{EI}{\rho A}}\sqrt{1+\frac{P_0 L^2}{\gamma EI}} \tag{9}$$

where the coefficients c and γ depend on the boundary conditions. Table 1 collects their values for several boundary conditions.

Equation (8) and hence (9) can also be used for axially constrained beams if transverse oscillations can be considered small with respect to the beam height. This hypothesis, which is often reasonable for structural problems at the macroscale, is in general not valid for microstructures as those of MEMS resonators. In this case the complete equation (7) and the associated boundary conditions should be considered.

2.2 Hamilton's principle

The nonlinear equilibrium equation (7) can also be obtained by the Hamilton's variational statement of dynamics. The Hamilton functional reads

$$\mathcal{H}\left(t\right) = \int_0^t \left[T - V\right] dt = \int_0^t \mathcal{L} dt \tag{10}$$

T being the kinetic energy, V the potential energy and $\mathcal{L} = T - V$ the Lagrange function. Neglecting the inertial effect in the axial direction the kinetic and potential energies are expressed

as

$$T(\dot{w}) = \frac{1}{2}\int_0^L \rho A \dot{w}^2 dx$$

$$V(w) = \frac{1}{2}\int_0^L EI\left(w''\right)^2 dx + \frac{1}{2}\frac{k_a EA}{k_a L + EA}\left[\int_0^L \frac{1}{2}\left(w'\right)^2 dx\right]^2 + P_0 \int_0^L \frac{1}{2}\left(w'\right)^2 dx - \int_0^L qw dx \tag{11}$$

The Hamilton's principle states that the real motion makes stationary the Hamiltonian functional increment for any varied path δw from time t_1 and t_2 with $\delta w(t_1) = \delta w(t_2) = 0$, i.e.

$$\delta \int_{t_1}^{t_2} \left[T(\dot{w}) - V(w)\right] dt = 0 \tag{12}$$

Integrating by parts in time the first term one obtains

$$\delta \int_{t_1}^{t_2} T(\dot{w})\, dt = \int_{t_1}^{t_2} \delta T dt = -\int_{t_1}^{t_2}\int_0^L \rho A \ddot{w} \delta w dx dt \tag{13}$$

The second term in (12) can be developed as

$$\delta \int_{t_1}^{t_2} V(w)\, dt = \int_{t_1}^{t_2} \delta V dt =$$

$$\int_{t_1}^{t_2}\left[\int_0^L \left(EIw''\right)\delta w'' dx + \frac{k_a EA}{k_a L + EA}\int_0^L \frac{1}{2}\left(w'\right)^2 dx \int_0^L w'\delta w' dx + P_0 \int_0^L w'\delta w' dx - \int_0^L q\delta w dx\right] dt \tag{14}$$

Integrating by parts in space the variation δV one has

$$\delta V(w) = \left[\left(EIw''\right)\delta w'\right]_0^L - \left[\left(\left(EIw''\right)' - P_0 w' - \frac{k_a EA}{k_a L + EA}\int_0^L \frac{1}{2}\left(w'\right)^2 dx\; w'\right)\delta w\right]_0^L +$$

$$\int_0^L \left[\left(EIw''\right)'' - P_0 w'' - \frac{k_a EA}{k_a L + EA} w'' \int_0^L \frac{1}{2}\left(w'\right)^2 dx - q\right]\; \delta w dx \tag{15}$$

Substituting Eqs. (13) and (15) into Eq. (12) one finally obtains the equation

$$-\int_{t_1}^{t_2}\int_0^L \left[\rho A\ddot{w} + \left(EIw''\right)'' - P_0 w'' - \frac{k_a EA}{k_a L + EA} w'' \int_0^L \frac{1}{2}\left(w'\right)^2 dx - q\right]\delta w dx\; dt$$

$$-\left[\left(EIw''\right)\delta w'\right]_0^L + \left[\left(\left(EIw''\right)' - P_0 w' - \frac{k_a EA}{k_a L + EA}\int_0^L \frac{1}{2}\left(w'\right)^2 dx\; w'\right)\delta w\right]_0^L = 0 \tag{16}$$

Since the variation δw is arbitrary Eq. (16) is equivalent to the dynamic equilibrium equation (7) with the boundary conditions

$$EIw'' = 0 \qquad or \qquad \delta w' = 0 \quad for\ x = 0, L$$

$$\left(EIw''\right)' - P_0 w' - \frac{k_a EA}{k_a L + EA}\int_0^L \frac{1}{2}\left(w'\right)^2 dx\; w' = 0 \qquad or \qquad \delta w = 0 \quad for\ x = 0, L$$

.

2.3 One degree of freedom approximation

Numerical solutions for the transversal oscillation of the nonlinear beam can be obtained expressing w in terms of a set of n generalized coordinate $Z_i(t)$ multiplied by known space functions $\Psi_i(x)$, substituting it into the kinetic and potential energies and using the Hamilton's principle to obtain the Lagrange equations of motion

$$\frac{d}{dt}\frac{\partial \mathcal{L}}{\partial \dot{Z}_i} - \frac{\partial \mathcal{L}}{\partial Z_i} = 0 \qquad i = 1, .., n$$

In the spirit of the Rayleigh method a single generalized variable $Z(t)$ can be introduced and the approximate solution for the transversal oscillation of a nonlinear beam can be searched in the form

$$w(x,t) = Z(t)\Psi(x) \tag{17}$$

$\Psi(x)$ being the eigenfunction of the same problem without second order effects. Considering free oscillations ($q = 0$), the approximate Lagrangian function reads

$$\begin{aligned}\mathcal{L}\left(\dot{Z}, Z\right) = &\frac{1}{2}\dot{Z}^2 \int_0^L \rho A \Psi^2 dx - \frac{1}{2} Z^2 \int_0^L EI\left(\Psi''\right)^2 dx \\ &- \frac{1}{2}\frac{k_a EA}{k_a L + EA} Z^4 \int_0^L \frac{\left(\Psi'\right)^2}{2} dx \int_0^L \frac{\left(\Psi'\right)^2}{2} dx - Z^2 P_0 \int_0^L \frac{\left(\Psi'\right)^2}{2} dx\end{aligned}$$

The corresponding Lagrange equation of motion is

$$m\ddot{Z} + k_1 Z + k_3 Z^3 = 0 \tag{18}$$

with

$$\begin{aligned} m &= \int_0^L \rho A \Psi^2 dx, \\ k_1 &= k_e + k_G, \; k_e = \int_0^L EI\left(\Psi''\right)^2 dx, \; k_G = P_0 \int_0^L \left(\Psi'\right)^2 dx, \\ k_3 &= \frac{1}{2}\frac{k_a EA}{k_a L + EA} \int_0^L \left(\Psi'\right)^2 dx \int_0^L \left(\Psi'\right)^2 dx \end{aligned} \tag{19}$$

Equation (18) is known as the Duffing oscillator equation for a single degree of freedom system, m is the equivalent mass, k_e is the equivalent linear elastic flexural stiffness, k_G is the generalized geometric stiffness due to a constant initial axial load and k_3 is the cubic nonlinear constant. For the problem under consideration of nonlinear oscillation of a single span beam k_3 given in Eq. (19) is always positive (hard spring effect). The solution of Eq. (18) can be obtained from series of successive approximations, see [7]

$$Z = Z^{(1)} + Z^{(2)} + Z^{(3)} \tag{20}$$

where

$$Z^{(1)} = A\ \cos\omega t,\ Z^{(2)} = 0,\quad Z^{(3)} = -\frac{A^3}{32}\frac{k_3}{k_1}\cos 3\omega t \tag{21}$$

In (21) A is the oscillation amplitude and ω is the actual value of the natural frequency which differs from the reference value of the linear case $\omega_0 = \sqrt{\frac{k_1}{m}}$. The natural frequency of the nonlinear problem can be expressed as

$$\omega = \omega_0\left(1 + \frac{3}{8}\frac{k_3}{k_1}A^2\right) \tag{22}$$

Note that, at difference from a linear oscillator, the fundamental frequency ω of the Duffing oscillator does depend on the oscillation amplitude A.

Nonlinearity also affects the forced oscillations of the system. Considering a harmonic driving term $f(t) = f\cos\Omega t$, of frequency Ω close to the natural frequency, neglecting damping, one obtains a relation between the amplitude f and the frequency Ω of the driving force and the amplitude A of the forced vibration of the beam (see e.g. [7])

$$\left(\frac{f}{k_1}\right)^2 = \left(2\left(1 - \frac{\Omega}{\omega_0}\right)A + \frac{3}{4}\frac{k_3}{k_1}A^3\right)^2 \tag{23}$$

The solution of equation (23) is shown in Figure 2 in terms of the dynamic amplification factor $A/\frac{f}{k_1}$ versus the ratio $\frac{\Omega}{\omega_0}$ between the frequency of the driving force Ω and the reference natural frequency ω_0. For $k_3 > 0$, the resonance curve is bent towards the high frequencies and there are three solutions for sufficiently high frequencies. Two solutions are stable while the third belongs to an unstable branch, dotted in Figure 2.

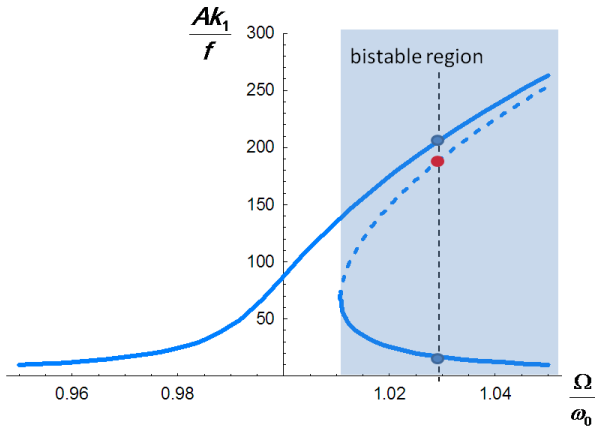

Figure 2: Forced frequency response of nonlinear resonator: normalized dynamic amplification factor vs. normalized frequency.

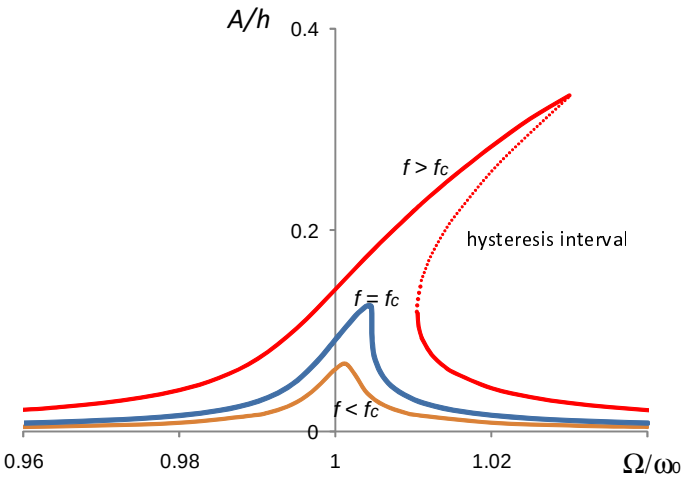

Figure 3: Resonance curves in the nonlinear region, accounting for damping, for different excitation amplitude f.

When also damping is considered the response becomes a multi-valued function of the frequency, in some finite frequency range, only above a critical excitation amplitude f_c. Figure 3 shows typical responses for $f \lessgtr f_c$ in terms of oscillation amplitude, normalized with the beam thickness h, versus normalized frequency $\frac{\Omega}{\omega_0}$. In all cases the resonant frequency is shifted upwards but for $f < f_c$ hysteresis phenomena due to the multi-valued response are avoided. Even though usually resonating devices are designed to have a hysteresis-free response there are some applications in which the nonlinear bistable regime is attained, see e.g. [2].

A more general form of the nonlinear dynamic equilibrium equation for a single degree of freedom oscillator also includes a second order term in Z

$$m\ddot{Z} + k_1 Z + k_2 Z^2 + k_3 Z^3 = 0 \tag{24}$$

Note that in capacitive microresonators the quadratic term can arise from electrostatic nonlinearities as discussed in [6] but it can also be present as a consequence of a slightly different geometry of the resonator, as it will be shown in Section 3.2.

The solution of Eq. (24) is still given by Eq. (20) with

$$Z^{(1)} = A\ \cos\omega t,\ Z^{(2)} = 0,\quad Z^{(3)} = \frac{A^3}{16}\left(\frac{1}{3}\left(\frac{k_2}{k_1}\right)^2 - \frac{k_3}{2k_1}\right)\cos 3\omega t \tag{25}$$

$$\omega = \omega_0\left[1 + \left(\frac{3}{8}\frac{k_3}{k_1} - \frac{5}{12}\left(\frac{k_2}{k_1}\right)^2\right)A^2\right] \tag{26}$$

As for the oscillation response driven by a force $f(t) = f\cos\Omega t$, the following relation holds instead of (23)

$$\left(\frac{f}{k_1}\right)^2 = \left[2\left(1-\frac{\Omega}{\omega_0}\right)A + \left(\frac{3}{4}\frac{k_3}{k_1} - \frac{5}{6}\left(\frac{k_2}{k_1}\right)^2\right)A^3\right]^2 \tag{27}$$

Depending on the values of the stiffness constants k_1, k_2 and k_3, different frequency response curves can be obtained, namely one can have three solutions for some $\frac{\Omega}{\omega_0} < 1$ (soft spring effect), one solution for all $\frac{\Omega}{\omega_0}$ or three solutions for some $\frac{\Omega}{\omega_0} > 1$ (hard spring effect). Figure 4 shows the behavior of a resonator with $k_3 > 0$, for varying ratio $\frac{k_2 L}{k_1}$. Note that from (27) if $k_3 = \frac{10}{9}\frac{{k_2}^2}{k_1}$ the coefficient of A^3 vanishes in Eq. (27) and the frequency response curve of a linear oscillator is recovered. For a real system with damping, the dynamic magnification factor $A/\frac{f}{k_1}$ is limited and there is a range of values of k_1, k_2 and k_3 for which a unique solution is obtained. This feature is very important in real resonators as will be discussed in the following section.

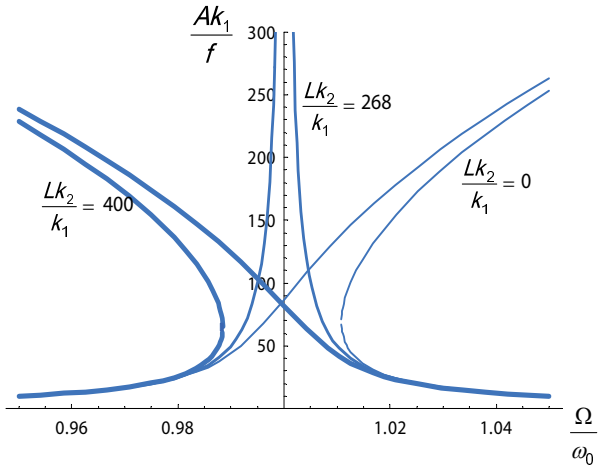

Figure 4: Forced frequency response of nonlinear resonator for varying stiffness ratio $\frac{Lk_2}{k_1}$: normalized dynamic amplification factor vs. normalized frequency.

3 Capacitive nonlinear microresonators

3.1 Doubly clamped resonator

As a first example consider the silicon resonator schematically shown in Figure 5, of length $L = 400\mu m$ and cross section $1.2\mu m \times 15\mu m$. The resonator is doubly clamped and it is excited by an electrode (parallel plate scheme with a gap $g = 2.1\mu m$). In the following this resonator will be referred to as "I-shaped" resonator.

A coupled electromechanical analysis has been performed in order to compute the axial force induced in the beam for different levels of the voltage applied to the electrode. Both the beam and the dielectric medium between the electrodes should be discretized to compute the electric field and the corresponding mechanical response of the resonator. Since large displacements are considered, the electrostatic problem should be solved on a varying domain, considering the deformed mesh. A detail of the adopted discretization is shown in Figure 5. The electric force makes the beam oscillating and induces a axial tensile force in the beam: Figure 6 shows the axial force in the beam for increasing values of the maximum oscillation at the center C of the beam $w_{\max}\left(\frac{L}{2}\right) = \max_t w\left(\frac{L}{2}, t\right)$.

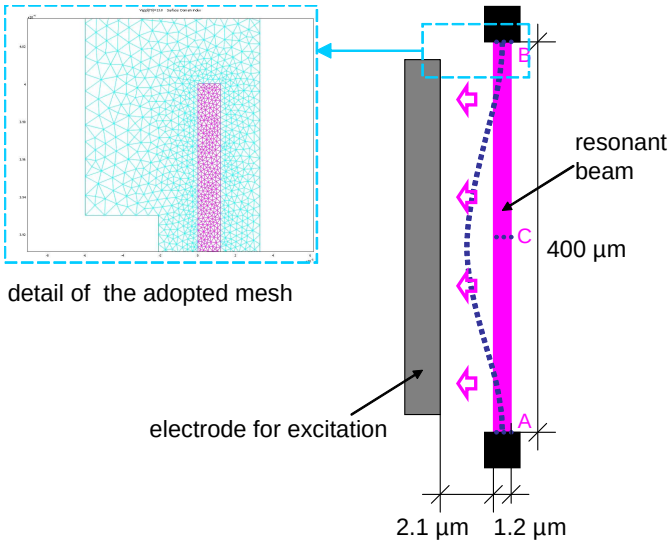

Figure 5: Geometry and discretization of the capacitive "I-shaped", doubly clamped resonator

An analytical prediction of the axial force can be obtained from the nonlinear dynamic beam theory previously presented with the single degree of freedom approximation. To this purpose we set $P_0 = 0$ and we introduce the approximate solution (17) into Eq. (6), choosing for $\Psi(x)$ the eigenfunction of the doubly clamped linear beam, normalized so that $\Psi\left(\frac{L}{2}\right) = 1$, i.e.

$$\Psi = \frac{1}{1.588}\left[\cos\left(4.73\frac{x}{L}\right) - \cosh\left(4.73\frac{x}{L}\right) - 0.9825(\sin\left(4.73\frac{x}{L}\right) - \sinh\left(4.73\frac{x}{L}\right))\right] \tag{28}$$

Assuming the Young's modulus $E = 150$ GPa for the silicon, the resulting axial force is (using IS units, with Z expressed in meters)

$$N(t) = 41.15 \times 10^6 \; Z(t)^2$$

This analytical estimate, also plotted in Figure 6, is in very good agreement with the numerical results. It should be noted that this geometry of the resonator, which is representative of

silicon resonators fabricated by surface micromachining results in relative high axial force (some micronewton for a maximum oscillation of tenths of micron) implying a significant nonlinear behavior.

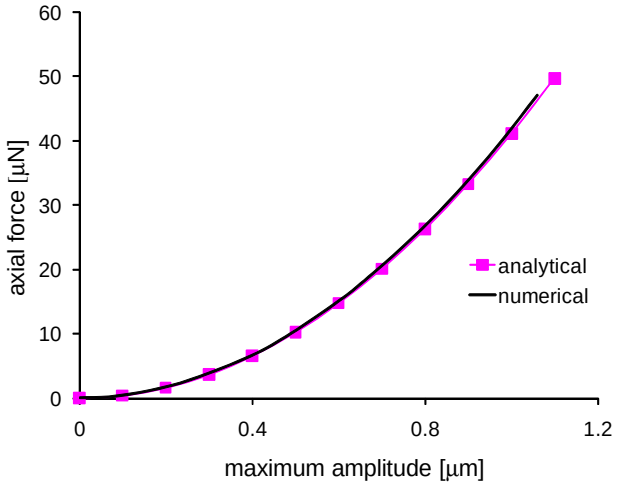

Figure 6: Axial force versus maximun displacement of the mid point for the "I-shaped" resonator

3.2 "L-shaped" resonator

A completely different behavior can be obtained by slightly changing the resonator geometry adding a short arm A-B of length a, as shown in Figure 7. This resonator will be called "L-shaped" resonator. In this case the transversal electrostatic force produces a axial force in the resonant beam also when second order effects are neglected. This additional contribution to the axial force linearly depends on the applied electrostatic force and hence on the oscillation of the central point $w\left(\frac{L}{2},t\right)$, or, in the single degree of freedom approximation, on the coordinate $Z\left(t\right)$. A simple scheme for the evaluation of the axial force at the first order, $N_1\left(t\right)$, is shown in Figure 8. The transversal load q represents the electric force induced by the applied voltage; this force is uniformly distributed only in the ideal case of a parallel plate with uniform gap between the electrodes. The actual distribution is non-uniform due to the beam deformation. Figure 9 shows the variation of the electric force along the resonator for increasing values of applied voltage: for low voltage an almost uniform distribution is obtained while for high voltage there is a significant variation of the intensity along the bar. Assuming in a first approximation a uniform q and using the linear Bernoulli beam theory, standard calculation gives

$$N_1 = qL\frac{\alpha^2\left(24\alpha\beta-1\right)}{8\left(1+\alpha\right)\left(3\beta+9\alpha\beta+36\alpha\beta^2-9\alpha^2\beta+\alpha^3+9\alpha^3\beta+3\alpha^4\beta\right)} \tag{29}$$

with $\alpha = \frac{a}{L}$ and $\beta = \frac{I}{AL^2}$. Since the amplitude of the oscillation is proportional to the applied load q, one can conclude that the first order axial force is proportional to the amplitude Z through a coefficient F only depending on the geometrical properties α, β and L

$$N_1(t) = F(\alpha, \beta, L)\ Z(t) \tag{30}$$

Including also the second order effect the 1D oscillator equivalent to the "L-shaped" resonator turns out to be governed by the Eq. (24), with k_2 related to F.

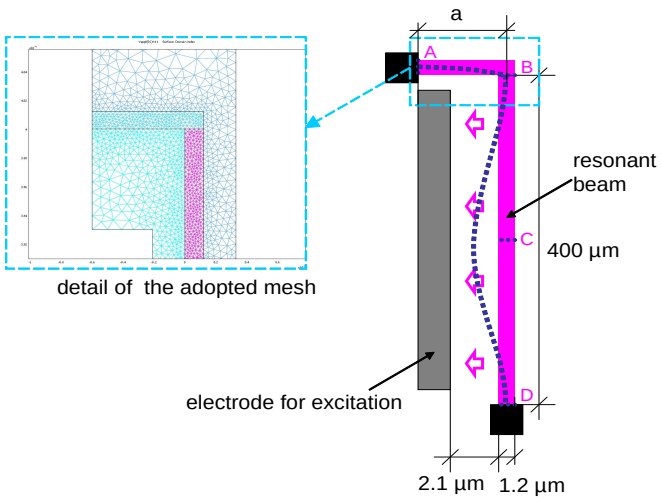

Figure 7: Geometry and discretization of the "L- shaped", doubly clamped resonator

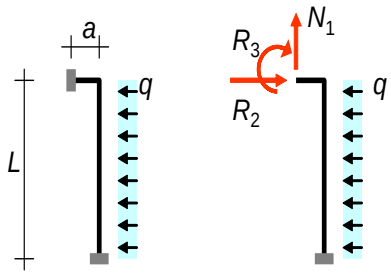

Figure 8: "L-shaped" resonator: scheme for the evaluation of the axial force (first order)

The finite element simulation allows to compute the axial force in the resonator for increasing oscillation. Results are shown in Figure 10, bold line. An analytical approximation can be obtained adding to the first order term computed according to Eq. (30) the second order term given by Eq. (6), with a suitable value of the axial-spring stiffness k_a. This spring should

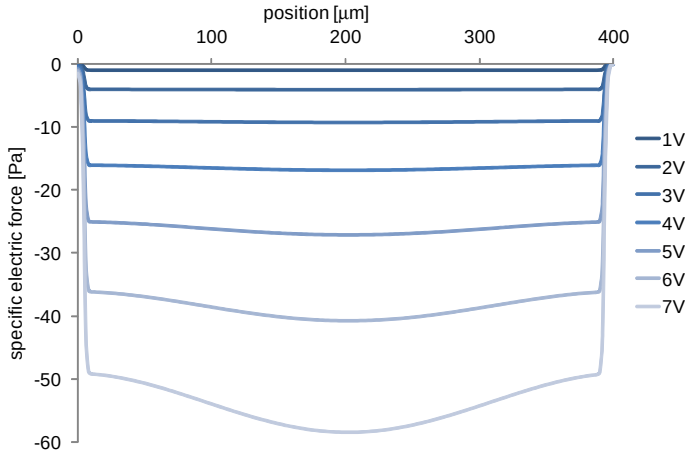

Figure 9: Distribution of the electric force along the resonator for varying applied voltage

represent the axial constraint given by the part A-B to the resonator B-D. The value of k_a can be bounded by the values $k_a = \frac{3EI}{a^3}$ and $k_a = \frac{12EI}{a^3}$, corresponding respectively, to free rotation and to zero rotation of node B. The analytical estimates of axial force obtained with this two extreme values are also shown in Figure 10: a reasonable prediction is obtained with the free rotation hypothesis.

For this geometry of the resonator the axial force is initially of compression due to the first order term, then, for high values of oscillation amplitude, the nonlinear tension term becomes predominant. In all the considered range of displacement the axial force turns out to be significantly smaller than the one obtained for the "I-shaped" resonator and there is a value of the oscillation for which the axial force vanishes. This feature is very important since one can tune the actuation voltage amplitude in such a way that the axial force vanishes and the oscillator response can be considered as linear. Figure 11 shows the deformed configuration obtained by the finite element analysis with the contour plot of the vertical stress from which the axial force has been computed.

4 Conclusions

The contribution of non-linear terms in the equation of motion drastically change the dynamic behavior of resonating slender beams especially when their size is reduced. To push the limits of the linear behavior a "L-shaped" capacitive silicon resonator has been proposed. Both analytical and numerical analyses show that this geometry, coupled with a proper choice of the actuation voltage, can effectively reduce the effect of nonlinearities. The use of this microresonator in acceleration sensing is currently under study.

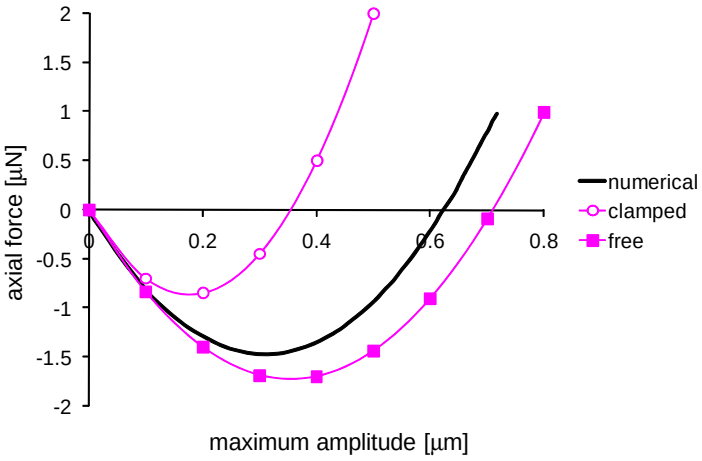

Figure 10: "L-shaped" resonator: axial force versus maximum oscillation amplitude: numerical results and analitical prediction considering zero rotation or free rotation.

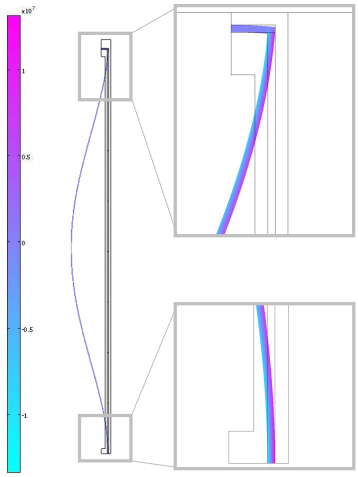

Figure 11: "L-shaped" resonator: controur plots of the vertical stress of the deformed configuration (amplification factor 50) and detail of the boundary conditions.

Acknowledgement

The author wish to thank Dr. L. Domenella for his assistance in numerical simulations. Financial support of the Cariplo foundation 2007 project: "Dissipative and failure phenomena in Micro and Nano Electro Mechanical Systems" is gratefully acknowledged.

References

[1] M. Aikele, K. Bauer, W. Ficker, F. Neubauer, U. Prechtel, J. Schalk, and H. Seidel. Resonant accelerometer with self-test. *Sensors and Actuators A*, 92:161–167, 2001.

[2] R. Almog, S. Zaitsev, O. Shtempluck, and E. Buks. Signal amplification in a nanomechanical duffing resonator via stochastic resonance. *Appl. Phys. Lett.*, 90, 2007.

[3] A. Bokaian. Natural frequencies of beams under tensile axial load. *J. of Sound and Vibration*, 142(3):481–498, 1990.

[4] M. Esashi. Resonant sensors by silicon micromachining. In *Proc. 1996 IEEE International frequency control symposium*, pages 609–614, 1996.

[5] V. Ferrari, A. Ghisla, D. Marioli, and A. Taroni. Silicon resonant accelerometer with electronic compensation of input-output cross-talk. *Sensors and actuators A*, 123-124:258–266, 2005.

[6] V. Kaajakari, T. Mattila, A. Oja, and H.Seppa. Nonlinear limits for single-crystal silicon microresonators. *J. MEMS*, 13(5), 2004.

[7] L. D. Landau and E. M. Lifsic. *Meccanica*. Boringhieri, 1965.

[8] A. A. Seshia, M. Palaniapan, T. A. Roessig, R. T. Howe, and S. Montague R. W. Gooch, T. R. Schimert. A vacuum packaged micromachined resonant accelerometer. *J. MEMS*, 11(6):784–793, 2002.

[9] W. Stokey. Vibration of systems having distributed mass and elasticity. In C. Harris, editor, *Shock and vibration handbook*. McGraw-Hill, 1988.

[10] J. A. Wickert. Non-linear vibration of traveling tensioned beam. *Int. J. Non-Linear Mechanics*, 27(3):503–517, 1992.

[11] J. D. Zook, D. W. Burns, H. Gueckel, J. J. Sniegowski, R. L. Engelstad, and Z. Feng. *Resonant microbeam strain transducers, Transducers 91, IEEE 91CH2817-5*. IEEE Publishing Services, New York.